Broadband vibration damping of non-periodic plates by piezoelectric coupling to their electrical analogues

Robin Darleux, Boris Lossouarn, Jean-François Deü

Broadband vibration damping of non-periodic plates by piezoelectric coupling to their electrical analogues

R. Darleux, B. Lossouarn*, J.-F. Deü

Laboratoire de Mécanique des Structures et des Systèmes Couplés (LMSSC)
Conservatoire national des arts et métiers (Cnam)
292 rue Saint-Martin, 75003 Paris, France

Abstract

Several solutions for multimodal vibration damping of thin mechanical structures based on piezoelectric coupling have been developed over the years. Among them, piezoelectric network damping consists in using piezoelectric transducers to couple a structure to an electrical network, where the transferred electrical energy can be dissipated. In particular, the effectiveness of coupling rods, beams and plates to their analogous electrical networks has been proven. This work is the first step going towards more complex structures. After defining and experimentally validating a fully passive electrical analogous network of a simply-supported plate, the study is extended to the damping of a non-periodic plate. The non-periodicities here studied include the addition of a local mass and a variable thickness. Numerical simulations and experiments show that in these cases, a broadband damping is achieved once the piezoelectric transducers are coupled to an adequate analogous network. A finite element model of the structure coupled to a 2D non-periodic electrical network is concurrently developed and validated, which is another contribution of the present work.

Keywords: Vibration mitigation, Multimodal damping, Piezoelectric coupling, Direct electromechanical analogy, Finite element model, Passive network

1. Introduction

Damping of mechanical vibrations using piezoelectric coupling goes back to the 1990s, when the resonant shunt was described by Hagood and Von Flotow [1]. The efficiency of the resonant shunt to control a single mode of vibration has been extensively studied [2, 3]. The concept of piezoelectric shunt damping has then been extended to multimodal damping. Some passive solutions consider connecting a multi-branch shunt to a single piezoelectric transducer [4–7]. While adding only one piezoelectric transducer to the structure is barely intrusive, its position and dimensions cannot simultaneously maximize the electromechanical coupling for all modes [8]. As a result, the damping performance might be limited. Moreover, the required inductive components could be difficult to produce [9], and the number of involved electrical components may greatly increase with the number of modes to be controlled [7]. Another solution could use several independent piezoelectric transducers, each one being shunted in order to damp one particular mode of the structure [10, 11]. However, the resulting electromechanical coupling coefficients are inferior to the ones that would be induced by interconnecting all piezoelectric transducers.

Hence, the principle of piezoelectric network damping emerged in the early 2000s [12–15]. Broadband damping is achieved by bounding piezoelectric patches on a vibrating structure and interconnecting them with electrical components [16]. This way, the inductance requirements are reduced [13]. Besides, the topology of the network to be connected to the plate has a significant impact on the attainable damping

*Corresponding author
Email address: boris.lossouarn@lecnam.net (B. Lossouarn)

performance. It has been shown that connecting the vibrating structure to a network that has the same modal characteristics ensures that there is as much electrical energy as mechanical energy involved in the coupled system [12]. For this reason, the electrical analogues of mechanical structures have been revived for vibration mitigation purposes [17].

One way to define electrical analogues is to use an electromechanical analogy [18, 19]. Electrical analogues of beams and plates have been defined dating back to the early 1950s [20–22]. More recently, piezoelectric network damping of beams [23–25] and plates [26, 27] has been studied. Most of these works are based on the application of the force-current and velocity-voltage analogy, also called indirect analogy. In the present article, the force-voltage and velocity-current analogy, also called direct electromechanical analogy, is applied. Indeed, this analogy allows representing the electromechanical converter of a coupled system with passive electrical components when this converter uses the action of electrostatic forces [18]. Therefore, it is a convenient analogy to use to passively represent the piezoelectric coupling. As a consequence, one can derive a fully passive representation of a mechanical structure being coupled to an electrical network via piezoelectric transducers. The resulting electrical analogues have been implemented recently for the vibration mitigation of beams [28] and plates [29, 30]. Based on these recent articles, a plate electrical analogue is defined in section 2 of the present work, and a new network is produced for further measurements. The validation of the network is made by comparing measurements to simulations and by conducting an experimental modal analysis, which has not been done in the previous articles.

The main objective is to investigate the multimodal damping of complex structures coupled to their electrical analogues. This begins with the study of non-periodic plates. Since experimental setups will not be developed for all future numerical examples, having a predictive model of the behavior of a structure being coupled to an electrical network becomes necessary. Such a model could be used to find out the limits of the analogy between the structure and its electrical analogue. It could also be used to design the optimal dissipative components to insert in the network to obtain an optimized damping performance. The dynamics of complex 3D structures at low frequencies can adequately be forecast by the finite element method, on which the scientific literature is abundant [31, 32]. Our bibliography on the subject is not exhaustive, as it is not the aim of this article. The work of Thomas et al. [33] concerning a structure covered by thin piezoelectric patches is taken as the starting point. The main originality of their work is to consider only one electrical degree of freedom by piezoelectric patch, as they impose the equipotentiality in the electrodes. Thus, it is convenient to couple this finite element formulation to lumped electrical models, such as a network. In section 3, the main hypotheses to obtain this finite element formulation are recalled. The coupling of the vibrating structure to a 2D electrical network is then taken into account which is another contribution of this work. The resulting coupled model is validated by comparison with experimental results on a plate coupled to the previously produced electrical network.

The broadband damping of a periodic plate is addressed in section 4. The network is validated by comparing its electrical current mode shapes to velocity mode shapes of the plate. The coupled model developed in the previous section is then validated by comparing experimental results to simulated ones. Finally, two cases of non-periodic plates are highlighted in section 5. A mass is added on the first non-periodic plate to break its symmetry, while the second example is a plate of variable thickness. In both cases, the designed electrical analogues are validated by comparison of electrical and mechanical mode shapes, and passive broadband damping is achieved. These promising results extend the concept of passive vibration control by piezoelectric network damping to complex structures.

2. Plate electrical analogue

In this section, the electrical analogue of a square plate is assembled to produce a plate electrical analogue. A network model is then developed and validated. The validation is conducted by comparing the numerical and experimental frequency response functions (FRFs) and mode shapes of the analogous electrical network.

2.1. Design of a plate electrical analogue

The first step in defining a plate electrical analogue is to develop a discrete model of the mechanical structure. This model can be obtained by applying a finite difference scheme to the dynamics equation of a

Table 1: Direct electromechanical analogy.

Mechanical quantities		Electrical quantities
Force -Q		Voltage V_w
Moment -M		Voltage V_θ
Linear velocity $\dot{w}$		Electrical current $\dot{q}_w$
Angular velocity $\dot{\theta}$	$\longleftrightarrow$	Electrical current $\dot{q}_\theta$
Compliance $1/K_\theta$		Capacitance C
Mass m		Inductance L
Lever arm $a/2$		Transformer ratio $\hat{a}/2$

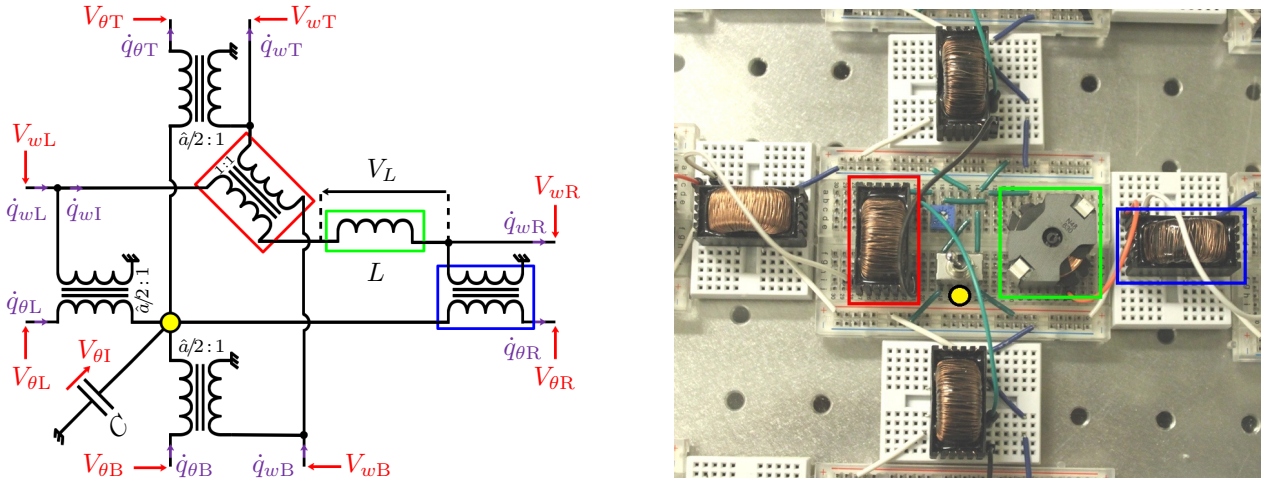

(a) (b)

Figure 1: (a) Scheme and (b) picture of the electrical analogue of a square plate, which highlight the central transformer in red, a side transformer in blue, the inductance in green, and the capacitance connection in yellow.

square plate. For a Kirchhoff-Love plate of thickness h, mass density ρ and bending stiffness K_θ in harmonic motion at angular frequency Ω, the considered equation is

$$K_\theta \left(\frac{\partial^4 w}{\partial x^4} + 2\frac{\partial^4 w}{\partial x^2 \partial y^2} + \frac{\partial^4 w}{\partial y^4} \right) = \rho h \Omega^2 w, \tag{1}$$

where w is the displacement in the direction normal to the plate, while x and y are the in-plane directions. The derivation of a discrete square plate model from equation (1) is detailed in [29, 30].

An electromechanical analogy [18, 19] is then applied to the resulting set of discrete mechanical equations. The indirect analogy, which states that velocities are analog to voltages and forces are analog to electrical currents, is considered in some works [20, 26]. In the present work, the direct electromechanical analogy is preferred, since it allows the fully passive representation of piezoelectric transducers [18]. Hence, the electrical analogue of a square plate is defined by replacing mechanical quantities in the developed discrete model by electrical quantities, according to the analogy in table 1. Therefore, figure 1a shows a scheme of the unit cell of the plate electrical analogue, which has already been exhibited in [29, 30]. The I, B, L, R and T subscripts on the electrical scheme in figure 1a refer to the central, bottom, left, right and top positions of the discretization grid, respectively. The electrical analogue of a rectangle plate can then be defined by assembling this unit cell along the x and y directions.

Besides, the boundary conditions of the plate should be reproduced in the electrical network. This network topology allows for direct equivalent electrical connections for the simply-supported and clamped

edges. Indeed, if for example the left edge of the unit cell is a boundary, then the simply-supported condition is equivalent to command that $V_{\theta \mathrm{L}} = 0$ and $\dot{q}_{w\mathrm{L}} = 0$, while the clamped condition is equivalent to command $\dot{q}_{\theta \mathrm{L}} = 0$ and $\dot{q}_{w\mathrm{L}} = 0$ [30].

Finally, the electrical components should be tuned so that the natural frequencies of the network are equal to the natural frequencies of the plate. This ensures identical bending wave propagation properties in the two media [29]. In this case, the frequential coherence condition is

$$\frac{1}{a^2}\frac{K_\theta}{m} = \frac{1}{\hat{a}^2}\frac{1}{LC}. \tag{2}$$

2.2. Model of the electrical network

Since the plate electrical analogue should be tested alone for validation, a lumped model of the entire network is developed. Using the notations in figure 1a, the values of the electrical charges and the voltages in one unit cell are denoted $\mathbf{q}_\mathrm{N}$ and $\mathbf{v}_\mathrm{N}$:

$$\mathbf{q}_\mathrm{N} = \left[\, q_{w\mathrm{B}} \;\; q_{\theta \mathrm{B}} \;\; q_{w\mathrm{L}} \;\; q_{\theta \mathrm{L}} \;\; q_{w\mathrm{R}} \;\; q_{\theta \mathrm{R}} \;\; q_{w\mathrm{T}} \;\; q_{\theta \mathrm{T}} \,\right]^\mathrm{T}, \tag{3a}$$

$$\mathbf{v}_\mathrm{N} = \left[\, V_{w\mathrm{B}} \;\; V_{\theta \mathrm{B}} \;\; V_{w\mathrm{L}} \;\; V_{\theta \mathrm{L}} \;\; V_{w\mathrm{R}} \;\; V_{\theta \mathrm{R}} \;\; V_{w\mathrm{T}} \;\; V_{\theta \mathrm{T}} \,\right]^\mathrm{T}. \tag{3b}$$

These vectors are related by

$$\mathbf{v}_\mathrm{N} = \mathbf{M}_\mathrm{elm}\ddot{\mathbf{q}}_\mathrm{N} + \mathbf{D}_\mathrm{elm}\dot{\mathbf{q}}_\mathrm{N} + \mathbf{K}_\mathrm{elm}\mathbf{q}_\mathrm{N}, \tag{4}$$

with $\mathbf{M}_\mathrm{elm}$, $\mathbf{D}_\mathrm{elm}$ and $\mathbf{K}_\mathrm{elm}$ being respectively the elementary matrices of electrical "mass", electrical damping and electrical "stiffness". The full derivation of these matrices is not detailed, as more information is available in [30]. Let us just precise that all matrices depend on the transformer ratio $\hat{a}$. Moreover, $\mathbf{M}_\mathrm{elm}$ is a function of the inductance value L, $\mathbf{D}_\mathrm{elm}$ is a function of the series resistance of the inductors and the series resistance of the transformers, and $\mathbf{K}_\mathrm{elm}$ is a function of the capacitance C. Then, following an assembly process, the vectors $\mathbf{Q}_\mathrm{N}$ and $\mathbf{V}_\mathrm{N}$ which contain the values of electrical charges and external voltages in the entire network are related to each other by

$$\mathbf{V}_\mathrm{N} = \mathbf{M}_\mathrm{N}\ddot{\mathbf{Q}}_\mathrm{N} + \mathbf{D}_\mathrm{N}\dot{\mathbf{Q}}_\mathrm{N} + \mathbf{K}_\mathrm{N}\mathbf{Q}_\mathrm{N}, \tag{5}$$

with $\mathbf{M}_\mathrm{N}$, $\mathbf{D}_\mathrm{N}$ and $\mathbf{K}_\mathrm{N}$ being respectively the assembled matrices of electrical "mass", electrical damping and electrical "stiffness".

The objective is to develop the electrical analogue of an aluminum plate of dimensions $420 \times 360 \times 3$ mm^3. It is periodically covered with 42 square piezoelectric patches of dimensions $50 \times 50 \times 0.5$ mm^3. Hence, a network made of 42 identical unit cells has been assembled. The structure and its analogous network are pictured in figures 2a and 2b, respectively. A closer look at a unit cell is shown in figure 1b. The design method of the analogous network is the same as in [29, 30]. However, the present plate is simply-supported, while it was fully clamped in the previous articles. Besides, more piezoelectric patches are used to cover the plate surface in the present work. For this reason, the structure and its analogous network share the same modal properties over a wider frequency range.

Following the method suggested in [34], the inductors are made by winding 610 turns of 0.2 mm thick copper wire around a core of N48 ferrite material from Epcos TDK, whose nominal permeance is 630 nH. Then, the inductance of the produced components can be set from 240 mH to 270 mH thanks to an adjusting screw. The network testing is made with a nominal inductance of $L = 244$ mH. The nominal series resistance of the inductors is 13.7 Ω. Furthermore, the ratio of the transformers is $\hat{a} = 4$, and their nominal series resistance is 16.8 Ω when used with a 1:1 ratio. An inductor and several transformers are pictured in figure 1b. Finally, ceramic capacitors which have a nominal capacitance of 145 nF are used.

By analogy with an exciting external force, an external voltage is applied between two unit cells of the network. The voltage V_ex is applied through an isolation transformer of ratio k. This isolation transformer is circled in blue in figure 2b. At the same time, the voltage drop V_L across each inductor of the network is measured. The numerical FRFs V_L/kV_ex obtained using the model of equation (5) can thus be compared to measurements. As an example, a comparison is plotted in figure 3 for V_L measured in the framed unit

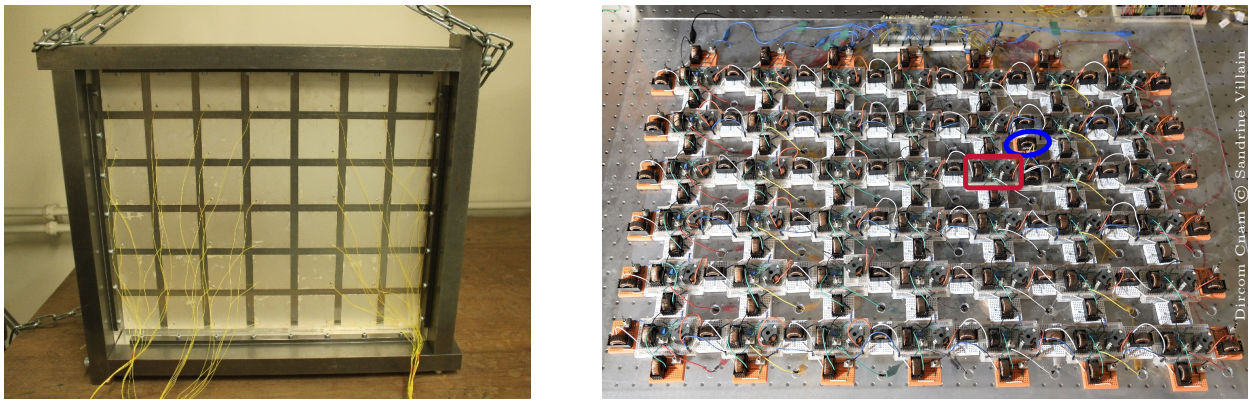

(a) (b)

Figure 2: (a) Plate covered with 42 piezoelectric patches and (b) its assembled analogous electrical network made of 42 unit cells. The isolation transformer for modal testing is circled in blue, while the unit cell on which the measurement in figure 3 is made is framed in red.

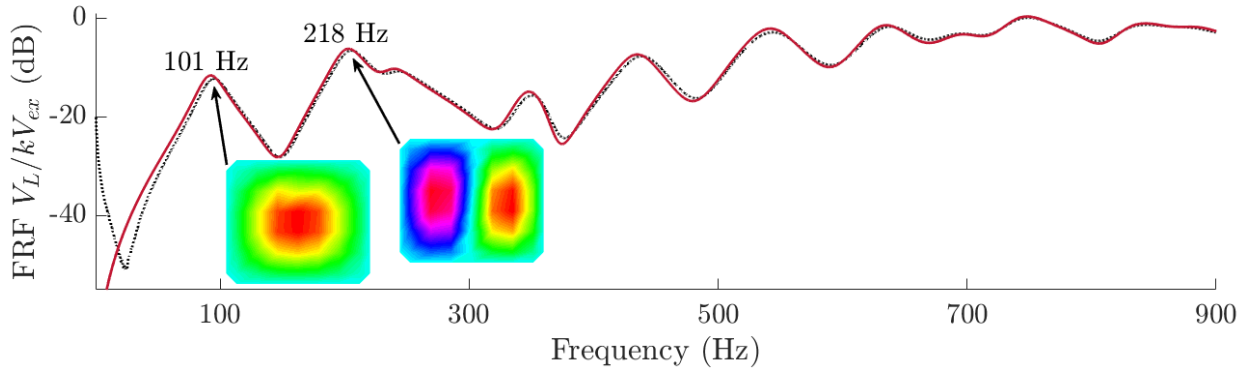

Figure 3: (⋯) Experimental and (—) simulated FRFs with V_L measured across the inductor of the unit cell framed in red in figure 2b. The operational electrical current shapes at the first two FRF peaks are highlighted.

cell in figure 2b. The simulated FRFs are in good agreement with the the measured ones. The remaining differences can be reduced by taking other parasitic elements of the transformers into account, such as the magnetizing branch and the winding capacitance. These kinds of refined models are not described here because the correlation between the proposed model and experiments is considered good enough to validate the network model from 50 Hz to 900 Hz.

Another validation of the developed model is to check if it has the same modal properties as the measurements. Visualizing the operational electrical current shapes is a first step in doing so. A couple of shapes at fixed frequencies are highlighted in figure 3, and one can attest they look like mode shapes of a simply-supported plate. To go further in the analysis, comparing the modeled electrical current mode shapes to the ones identified from measurements can be done using the modal assurance criterion (MAC) [35]. If the MAC matrix contains values close to 1, this means that the associated mode shapes are similar. On the other hand, low values in the MAC matrix are attained for two nearly orthogonal mode shapes. An experimental modal analysis of the network is performed by comparing the mode shapes of a mechanical structure and an electrical network using the MAC, which is an originality of the present work. The experimental mode shapes are extracted using the least-squares rational function estimation method suggested in [36]. The first fourteen experimental modes are identified between 50 Hz and 800 Hz, and therefore can be compared to simulated modes in figure 4. This MAC matrix shows that experimental and numerical modes are mutually

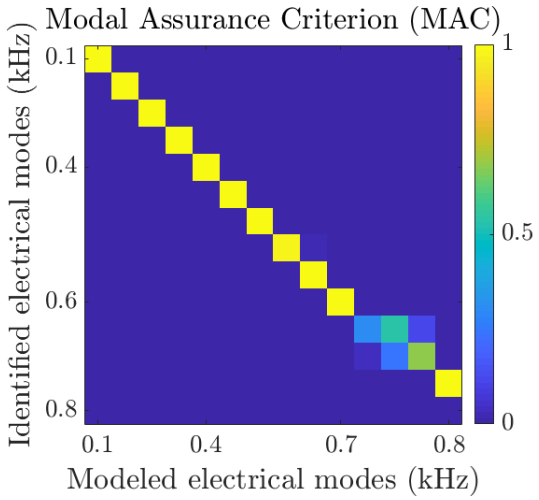

Figure 4: MAC matrix between experimental and simulated electrical current modes of the network.

consistent. The only problem is that the eleventh identified mode is a complex mode, whose real part is similar to the eleventh modeled mode, and whose imaginary part is similar to the twelfth modeled mode. This is due to significant and not purely proportional damping in the network. To conduct a complete experimental modal analysis would require refining the extraction of modes as well as the estimation of modal parameters. However, the developed model is deemed sufficiently precise to forecast the modal behavior of the electrical networks studied in the following sections.

3. Finite element model of a structure coupled to an electrical network

The main hypotheses to model the dynamics of a mechanical structure covered by piezoelectric patches are recalled. Then, the effect of the interconnections between patches via an electrical network is accounted for. The simulated results in the case of short-circuited piezoelectric patches are finally compared to experiments in order to validate the approach.

3.1. Finite element formulation

As stated in the introduction, the literature is abundant on finite element modeling of vibration damping by piezoelectric coupling [31, 32]. For the case of the plate covered with piezoelectric patches here studied, we chose to follow the method described by Thomas et al. in [33]. The main originality of this work is to include the voltage on the upper electrode of each piezoelectric patch as a global variable. Implementing the connection of the structure to lumped-element models of electronic circuits is then convenient. Though all equations are not detailed in the present paper, the main hypotheses to develop a finite element model of the structure are recalled.

The structure is modeled as an isotropic homogeneous linear elastic medium in which the piezoelectric coefficients vanish. The piezoelectric transducers exhibit transverse isotropic properties, and are polarized in their transverse directions. The patches thickness's are considered small when compared to their longitudinal dimensions. Under these assumptions, the derived equations of the variational formulation in terms of displacement and electric potential are then discretized. Following an assembly process, one obtains a finite element formulation of the coupled problem:

$$\begin{bmatrix} \mathbf{M_m} & \mathbf{0} \\ \mathbf{0} & \mathbf{0} \end{bmatrix} \begin{bmatrix} \ddot{\mathbf{U}} \\ \ddot{\mathbf{V}} \end{bmatrix} + \begin{bmatrix} \mathbf{D_m} & \mathbf{0} \\ \mathbf{0} & \mathbf{0} \end{bmatrix} \begin{bmatrix} \dot{\mathbf{U}} \\ \dot{\mathbf{V}} \end{bmatrix} + \begin{bmatrix} \mathbf{K_m} & \mathbf{K_c} \\ -\mathbf{K_c}^{\mathrm{T}} & \mathbf{K_e}^{-1} \end{bmatrix} \begin{bmatrix} \mathbf{U} \\ \mathbf{V} \end{bmatrix} = \begin{bmatrix} \mathbf{F} \\ \mathbf{Q} \end{bmatrix}, \tag{6}$$

Another equivalent formulation is to write the electrical equation with the electrical charges as state variables. Hence the equation (6) becomes

$$\begin{bmatrix} \mathbf{M_m} & \mathbf{0} \\ \mathbf{0} & \mathbf{0} \end{bmatrix} \begin{bmatrix} \ddot{\mathbf{U}} \\ \ddot{\mathbf{Q}} \end{bmatrix} + \begin{bmatrix} \mathbf{D_m} & \mathbf{0} \\ \mathbf{0} & \mathbf{0} \end{bmatrix} \begin{bmatrix} \dot{\mathbf{U}} \\ \dot{\mathbf{Q}} \end{bmatrix} + \begin{bmatrix} \mathbf{K_m} + \mathbf{K_c}\mathbf{K_e}\mathbf{K_c}^{\mathrm{T}} & \mathbf{K_c}\mathbf{K_e} \\ (\mathbf{K_c}\mathbf{K_e})^{\mathrm{T}} & \mathbf{K_e} \end{bmatrix} \begin{bmatrix} \mathbf{U} \\ \mathbf{Q} \end{bmatrix} = \begin{bmatrix} \mathbf{F} \\ \mathbf{V} \end{bmatrix}, \tag{7}$$

where $\mathbf{U}$ contains the nodal values of the displacement field $\mathbf{u}$ and $\mathbf{V}$ contains the voltage values $(V^{(1)}, \ldots, V^{(p)})$ on the upper electrodes of the piezoelectric patches. In $\mathbf{F}$ are the external mechanical forces applied to the structure, while in $\mathbf{Q}$ are the electrical charges $(Q^{(1)}, \ldots, Q^{(p)})$ on the upper electrodes of the piezoelectric patches. $\mathbf{K_c}$ is the coupling matrix. $\mathbf{M_m}$, $\mathbf{D_m}$ and $\mathbf{K_m}$ are the mechanical mass, damping and stiffness matrices, respectively. $\mathbf{K_e}$ is a diagonal matrix in which the j-th term is the inverse of the blocked piezoelectric capacitance $C^{\varepsilon(\mathrm{j})}$ of the j-th patch, which is

$$C^{\varepsilon(\mathrm{j})} = \frac{\epsilon_{33}{}^{\varepsilon} S^{(\mathrm{j})}}{h^{(\mathrm{j})}}, \tag{8}$$

where $S^{(\mathrm{j})}$ is the j-th patch surface area and $\epsilon_{33}^{\varepsilon}$ is the transverse permittivity of a piezoelectric medium with no strain. It represents the capacitance when no bending displacement is allowed.

3.2. Coupling of a structure to an electrical network

The piezoelectric patches bound to the structure are interconnected via the plate electrical analogue. The network can be considered as a passive electrical controller that commands a relationship between $\mathbf{V}$ and $\mathbf{Q}$. The goal is to relate $\mathbf{V}$ and $\mathbf{Q}$ to $\mathbf{V}_{\mathrm{N}}$ and $\mathbf{Q}_{\mathrm{N}}$ in order to take the influence of the network on the structure dynamics into account.

On one hand, the j-th element of $\mathbf{Q}$ is equal to the charge $q_{\theta\mathrm{B}}^{(\mathrm{j})} - q_{\theta\mathrm{T}}^{(\mathrm{j})} + q_{\theta\mathrm{L}}^{(\mathrm{j})} - q_{\theta\mathrm{R}}^{(\mathrm{j})}$ flowing through the capacitance $C^{\varepsilon(\mathrm{j})}$. This means that a matrix $\mathbf{P}$ can be assembled so that

$$\mathbf{Q} = \mathbf{P}\mathbf{Q}_{\mathrm{N}}. \tag{9}$$

On the other hand, the voltage vector $\mathbf{V}_{\mathrm{N}}$ is generated by the electrical currents flowing in the network and by the piezoelectric coupling with the vibrating structure. Firstly, let's consider that $\mathbf{U} \neq \mathbf{0}$ and $\mathbf{Q}_{\mathrm{N}} = \mathbf{0}$, leading to $\mathbf{Q} = \mathbf{0}$ and $\mathbf{q}_{\mathrm{N}} = \mathbf{0}$ for every unit cell. Then the scheme in figure 1a shows that $V_{w\mathrm{B}} = V_{w\mathrm{L}} = V_{w\mathrm{R}} = V_{w\mathrm{T}} = 0$ and that $V_{\theta\mathrm{B}} = V_{\theta\mathrm{L}} = V_{\theta\mathrm{R}} = V_{\theta\mathrm{T}} = V_{\theta\mathrm{I}}$. After an assembly process, one can show that $\mathbf{V}_{\mathrm{N}}$ and $\mathbf{V}$ are related by the same matrix $\mathbf{P}$ as in equation (9):

$$\mathbf{V}_{\mathrm{N}} = \mathbf{P}^{\mathrm{T}}\mathbf{V}. \tag{10}$$

Then, the electrical equation of the finite element formulation (7) with $\mathbf{Q} = \mathbf{0}$ is used to relate the voltage vector $\mathbf{V}_{\mathrm{N}}$ to the displacement field $\mathbf{U}$:

$$\mathbf{V}_{\mathrm{N}} = (\mathbf{K_c}\mathbf{K_e}\mathbf{P})^{\mathrm{T}}\,\mathbf{U}. \tag{11}$$

Let us then consider that $\mathbf{U} = \mathbf{0}$ while $\mathbf{Q}_{\mathrm{N}} \neq \mathbf{0}$. In the case of no piezoelectric coupling with the structure, it has been shown that the voltages and currents in the network are related by equation (5). The resulting expression of $\mathbf{V}_{\mathrm{N}}$ when $\mathbf{U} \neq \mathbf{0}$ and $\mathbf{Q}_{\mathrm{N}} \neq \mathbf{0}$ is derived by applying the superposition theorem with equations (5) and (11):

$$\mathbf{V}_{\mathrm{N}} = \mathbf{M}_{\mathrm{N}}\ddot{\mathbf{Q}}_{\mathrm{N}} + \mathbf{D}_{\mathrm{N}}\dot{\mathbf{Q}}_{\mathrm{N}} + \mathbf{K}_{\mathrm{N}}\mathbf{Q}_{\mathrm{N}} + (\mathbf{K_c}\mathbf{K_e}\mathbf{P})^{\mathrm{T}}\,\mathbf{U}. \tag{12}$$

Combining equations (7), (9) and (12) leads to a finite element formulation of a structure coupled to an electrical network:

$$\begin{bmatrix} \mathbf{M_m} & \mathbf{0} \\ \mathbf{0} & \mathbf{M}_{\mathrm{N}} \end{bmatrix} \begin{bmatrix} \ddot{\mathbf{U}} \\ \ddot{\mathbf{Q}}_{\mathrm{N}} \end{bmatrix} + \begin{bmatrix} \mathbf{D_m} & \mathbf{0} \\ \mathbf{0} & \mathbf{D}_{\mathrm{N}} \end{bmatrix} \begin{bmatrix} \dot{\mathbf{U}} \\ \dot{\mathbf{Q}}_{\mathrm{N}} \end{bmatrix} + \begin{bmatrix} \mathbf{K_m} + \mathbf{K_c}\mathbf{K_e}\mathbf{K_c}^{\mathrm{T}} & \mathbf{K_c}\mathbf{K_e}\mathbf{P} \\ (\mathbf{K_c}\mathbf{K_e}\mathbf{P})^{\mathrm{T}} & \mathbf{K}_{\mathrm{N}} \end{bmatrix} \begin{bmatrix} \mathbf{U} \\ \mathbf{Q}_{\mathrm{N}} \end{bmatrix} = \begin{bmatrix} \mathbf{F} \\ \mathbf{V}_{\mathrm{N}} \end{bmatrix}. \tag{13}$$

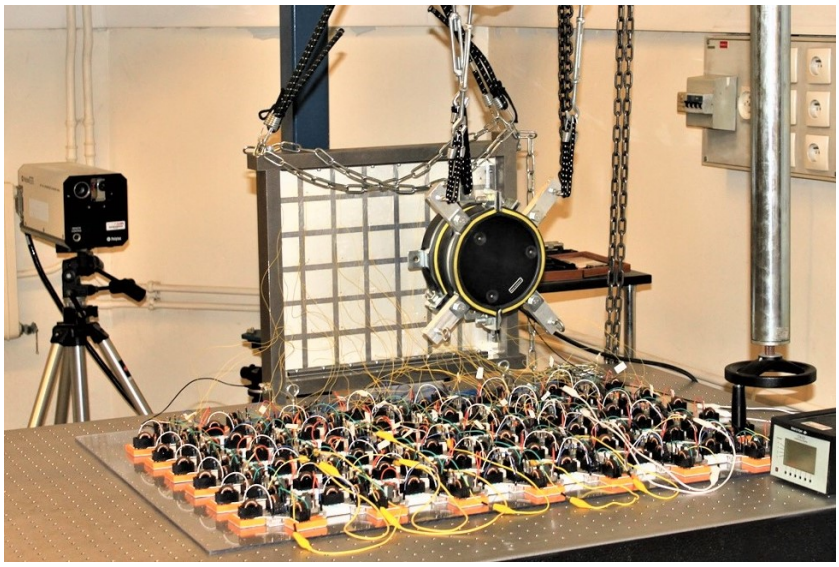

Figure 5: Picture of the setup, including the plate covered with piezoelectric transducers, a shaker, a laser vibrometer and the plate electrical analogue.

A similar expression is derived in [37] in the case of a single unit cell being periodically assembled along one direction. The present finite element formulation is an extension to non-periodic 2D networks. Besides, it is convenient as it allows to assemble the network unit cells the same way as in the finite element method. Hence, local modifications of network components can be implemented. This should ease the way going towards non-periodic structures.

3.3. Validation of the finite element model

Numerical simulations are compared to measurements to validate the finite element model developed in the previous subsections. The experimental setup is exhibited in figure 5. The simply-supported plate periodically covered with piezoelectric patches is suspended. A shaker applies a point load and a force transducer measures it. A laser vibrometer measures the velocity on the other side of the plate. The (x, y) location of both the excitation and the velocity measurements is drawn in figure 6. Moreover, the upper electrodes of the patches are either connected to the ground or to the network thanks to switches, one of which can be spotted in figure 1b.

The structure is modeled with 20-node hexahedral elements. Both the plate and the piezoelectric patches are meshed with one element in depth. In the other directions, the piezoelectric patches as well as the plate beneath them are meshed with $n_x \times n_y$ elements. Taking $n_x = n_y = 3$ leads to converged values for natural frequencies of the undamped structure up to 1 kHz. Accordingly, the figure 6 depicts the mesh used to obtain all the following numerical results.

The plate is made of duralumin. Its Poisson's ratio and density are respectively set at 0.346 and 2800 kg/m^3. Its Young's modulus is set at 68.8 GPa to adjust the eleventh natural frequency of the plate calculated with short-circuited piezoelectric patches to the corresponding resonance in the experimental measurement. This corresponds to the last peak before 900 Hz as plotted in figure 8. Structural damping is taken into account, so that the mechanical damping matrix $\mathbf{D_m}$ and the mechanical stiffness matrix $\mathbf{K_m}$ are related by

$$\mathbf{K_m} + \mathrm{j}\Omega\mathbf{D_m} = (1 + 2\mathrm{j}\xi)\,\mathbf{K_m}, \qquad \text{which is equivalent to} \qquad \mathbf{D_m} = \frac{2\xi}{\Omega}\mathbf{K_m}. \tag{14}$$

The damping coefficient ξ is set at 3.10^{-3} so that the amplitude of the first simulated peak is roughly equal to the measured one.

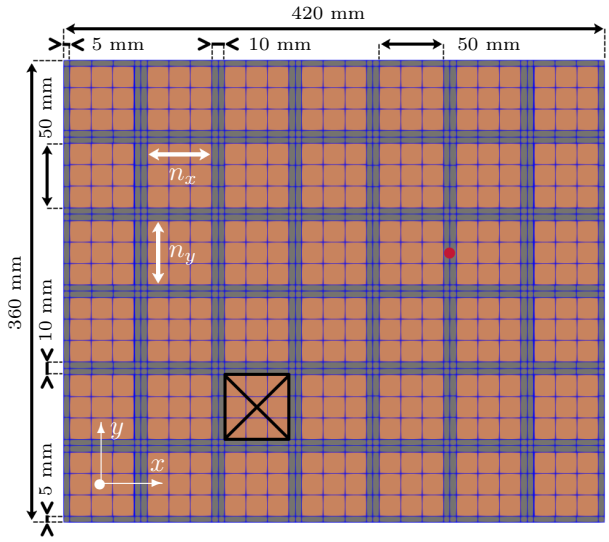

Figure 6: Dimensions and meshing of the mechanical structure, • (x, y) location of both the excitation and the velocity measurement, and ⊠ position of the added mass in section 5.1.

The piezoelectric patches are made of the PIC 153 PZT material [38]. Few material characteristics are available in the manufacturer's data. Thus these characteristics are either extrapolated from datasheets of other PZT materials, or numerically optimized. This is the case of the piezoelectric coefficients d_{31} and d_{33}. By extrapolation on the basis of other PZT materials whose characteristics are available in [38], it is assumed that $d_{33} \approx -2d_{31}$. Their values are then set in order to minimize the quadratic error on the coupling factors. The modal coupling factor $(k_c)_n$ for the n-th mode is

$$(k_c)_n = \sqrt{\left(\frac{(f_{\mathrm{OC}})_n}{(f_{\mathrm{SC}})_n}\right)^2 - 1}. \tag{15}$$

In this expression, $(f_{\mathrm{SC}})_n$ is the n-th normal frequency of the plate when the piezoelectric patches are short-circuited, while $(f_{\mathrm{OC}})_n$ is the n-th normal frequency of the plate when each upper electrode of the piezoelectric patches is left unconnected. Not interconnecting the upper electrodes of patches in the case of open-circuit allows to define a non-zero coupling factor for all modes, which leads to a more precise adjustment for the values of d_{33} and d_{31}. These frequencies are obtained by using the finite element formulation presented in equation (6). Computing the mean squared error (MSE) between simulated and measured values of $(k_c)_n$ for the first eleven modes of the structure results in figure 7a. As a consequence, the value of d_{31} is set at -260 pC/N and the value of d_{33} is estimated at 520 pC/N. This d_{33} value is notably smaller than the value of 600 pC/N indicated by the manufacturer's data. This confirms the need to experimentally evaluate the materials characteristics when possible.

As a result, the simulated coupling factors are shown in figure 7b. The gap between the simulated and measured coupling factors is less than 5 %. Besides, this maximum overestimation is for the first coupling factor and could be partly explained by the non-ideal experimental boundary conditions. The plate experimental setup is linked to a rigid frame via thin supports, while the plate is the only part of the assembly that is modeled. Therefore the added flexibility owned to the supports is not modeled. Knowing this maximum error of 5 % could be reduced, the prediction of the coupling factors is considered sufficiently precise. All numerical values which are needed for the modeling are summed up in table 2.

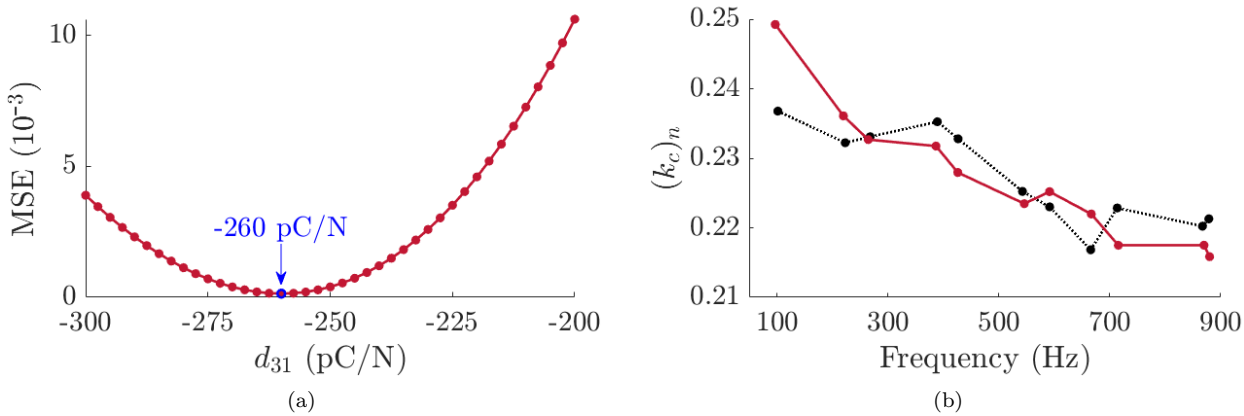

Figure 7: (a) MSE on the modal coupling factors for different d_{31} piezoelectric coefficient values and (b) resulting comparison between (···) measured and (—) simulated coupling factors of the first eleven plate modes.

Table 2: PIC 153 PZT material [38] characteristics which have been used for the finite element modeling.

Elastic coefficients (10^{-12}N/m^2)				Poisson coefficients (-)		Piezoelectric coefficients (10^{-12}C/N)		Relative permittivities (-)		Density (kg/m^3)	
s_{11}^E	16.83[a]	s_{33}^E	$1.15s_{11}^E$ [b]	ν_{12}	0.34	d_{31}	-260[c]	$\epsilon_{33}^\sigma/\epsilon_0$	4200	ρ_P	7600
s_{12}^E	$-\nu_{12}s_{11}^E$	s_{44}^E	$1.15s_{66}^E$ [b]	ν_{13}	$1.25\nu_{12}$ [b]	d_{33}	$-2d_{31}$ [b]	$\epsilon_{33}^\varepsilon/\epsilon_0$	2575[d]		
s_{13}^E	$-\nu_{13}s_{11}^E$	s_{66}^E	$2\left(s_{11}^E - s_{12}^E\right)$								

[a] Supposed equal to the s_{11}^E coefficient of the PIC 151 PZT material [38].
[b] Relations extrapolated from other PZT material characteristics.
[c] Set to minimize the MSE on the coupling factors (see figure 7a).
[d] Measured on an unbound depolarized patch at 1 kHz and low level of excitation.

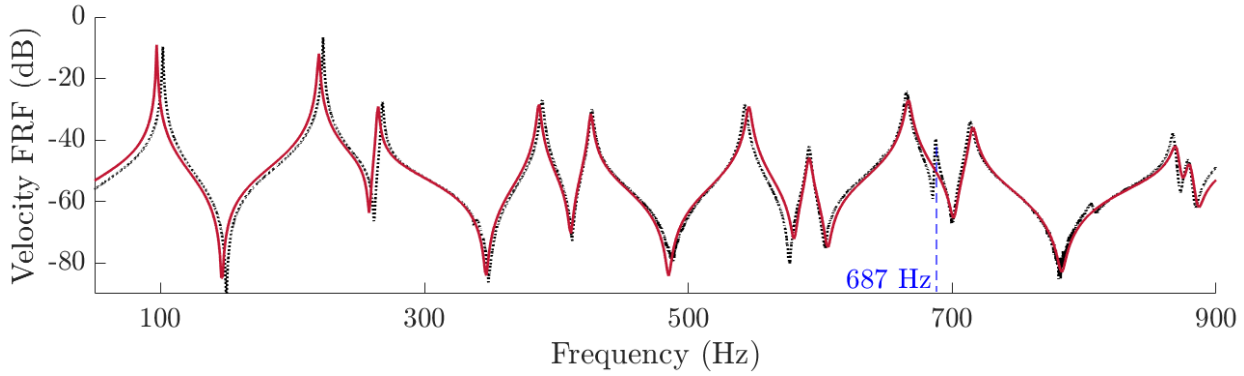

Figure 8: (···) Experimental and (—) simulated FRFs with short-circuited piezoelectric patches.

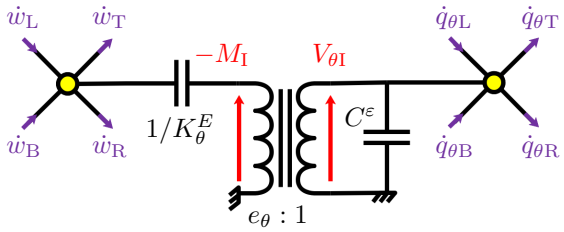

Figure 9: Electrical representation of the electromechanical coupling.

The case of short-circuited patches is simulated using the formulation of equation (6). The plotted results in figure 8 show that the numerical simulation forecasts the dynamics of the structure up to 900 Hz rather well. Moreover, the remaining differences between numerical and experimental results could be reduced. Indeed, the peak at 687 Hz can not be predicted by our model since it is a frame mode. Furthermore, the gaps between the first simulated and measured peaks can be attributed to the non-ideal experimental boundary conditions. This has been explained by Robin et al., who designed a first version of the setup in [39]. Other details are available in [40] as well.

4. Broadband damping of a periodic plate

The analogous network of a periodic plate is validated by comparing its natural frequencies and electrical current mode shapes to the natural frequencies and the velocity mode shapes of the mechanical structure. To do so, the nominal inductance value needed to meet the frequential coherence condition is estimated. Finally, vibration damping of the first modes of the structure is experimentally achieved by coupling the plate to its analogous network. A numerical simulation validates the model developed in section 3.2 of a structure being coupled to an electrical network.

4.1. Frequential coherence condition

In order to tune the natural frequencies of the network to the natural frequencies of the plate, the frequential coherence condition of equation (2) should be met. In the case of the periodic plate covered by piezoelectric patches, it becomes

$$\frac{1}{a^2}\frac{K_\theta^D}{m} = \frac{1}{\hat{a}^2}\frac{1}{LC^\varepsilon}. \tag{16}$$

In this last equation, K_θ^D is the mechanical stiffness when the piezoelectric patches are left in open-circuit. The blocked piezoelectric capacitance C^ε is the capacitance when no bending displacement is allowed. According to the lumped electrical model of the piezoelectric coupling [19], such as depicted in figure 9, these two quantities can be related to the mechanical stiffness when the piezoelectric patches are short-circuited and to the static piezoelectric capacitance, respectively denoted K_θ^E and C_0:

$$K_\theta^D = K_\theta^E + \frac{e_\theta^2}{C^\varepsilon}, \tag{17a}$$

$$C_0 = C^\varepsilon + \frac{e_\theta^2}{K_\theta^E}, \tag{17b}$$

with e_θ being the global coupling coefficient. From the two previous equations, one obtains

$$\frac{C^\varepsilon}{C_0} = \frac{K_\theta^E}{K_\theta^D}. \tag{18}$$

On that account, the frequential coherence condition of equation (16) can also be written

$$\frac{1}{a^2}\frac{K_\theta^E}{m} = \frac{1}{\hat{a}^2}\frac{1}{LC_0}. \tag{19}$$

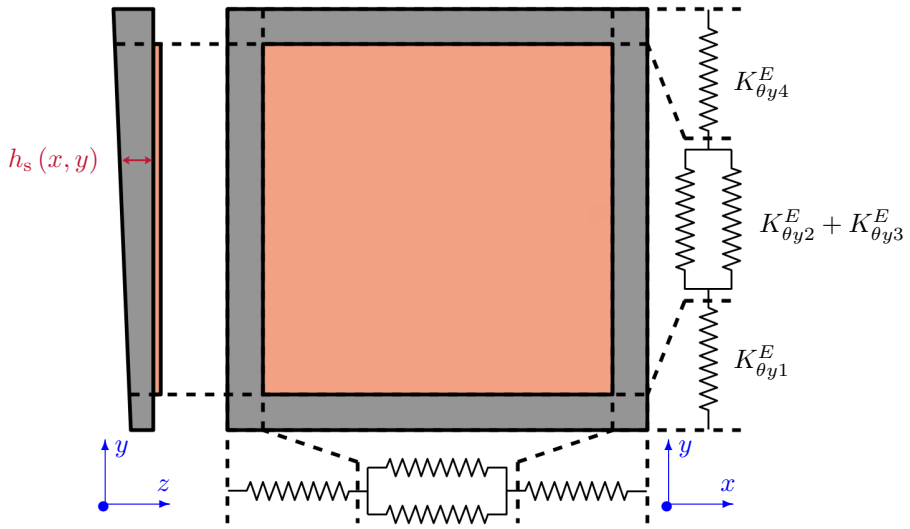

Figure 10: Square plate of variable thickness h_s covered by a square piezoelectric patch of constant thickness h_p. The stiffness of each portion of the plate and the piezoelectric patch can be modeled as a spring, such as drawn on the right hand-side. The represented thickness is not to scale.

The choice is to use the inductance value L as the tuning parameter. The side of the unit cell and the transformer ratio are set at $a = 60$ mm and $\hat{a} = 4$. The mass m values can be computed knowing the plate dimensions and the materials densities. This means that K^E_θ and C_0 should be estimated to obtain a value for L.

4.2. Estimation of the bending stiffness

The method of calculation of the bending stiffness value K^E_θ for a square mechanical plate is based on the model depicted in figure 10. It includes a series and parallel combination of discrete springs, so that the bending stiffness $K^E_{\theta y}$ when y is deemed as the normal axis is

$$\frac{1}{K^E_{\theta y}} = \frac{1}{K^E_{\theta y1}} + \frac{1}{K^E_{\theta y2} + K^E_{\theta y3}} + \frac{1}{K^E_{\theta y4}}, \tag{20}$$

where $K^E_{\theta y1}$, $K^E_{\theta y2}$ and $K^E_{\theta y4}$ are the stiffness of the plate portions indicated in figure 10, while $K^E_{\theta y3}$ is the stiffness of the piezoelectric patch. Denoting ν and Y the Poisson coefficient and the Young modulus of the plate, these stiffness values can be computed by the following expressions:

$$\frac{1}{K^E_{\theta y1}} = \frac{1-\nu^2}{Y} \int_0^{(a-l_\mathrm{p})/2} \frac{1}{I(y)}\, dy, \tag{21a}$$

$$\frac{1}{K^E_{\theta y2}} = \frac{1-\nu^2}{Y} \int_{(a-l_\mathrm{p})/2}^{(a+l_\mathrm{p})/2} \frac{1}{I(y)}\, dy, \tag{21b}$$

$$\frac{1}{K^E_{\theta y3}} = \frac{1-\nu_{12}^2}{1/s^E_{11}} \int_{(a-l_\mathrm{p})/2}^{(a+l_\mathrm{p})/2} \frac{1}{I_\mathrm{p}(y)}\, dy, \tag{21c}$$

$$\frac{1}{K^E_{\theta y4}} = \frac{1-\nu^2}{Y} \int_{(a+l_\mathrm{p})/2}^{a} \frac{1}{I(y)}\, dy, \tag{21d}$$

with I and I_p respectively being the second moments of area of the structure and of the piezoelectric patch. Assuming the piezoelectric patches thicknesses are small compared to the structure thickness, the expressions

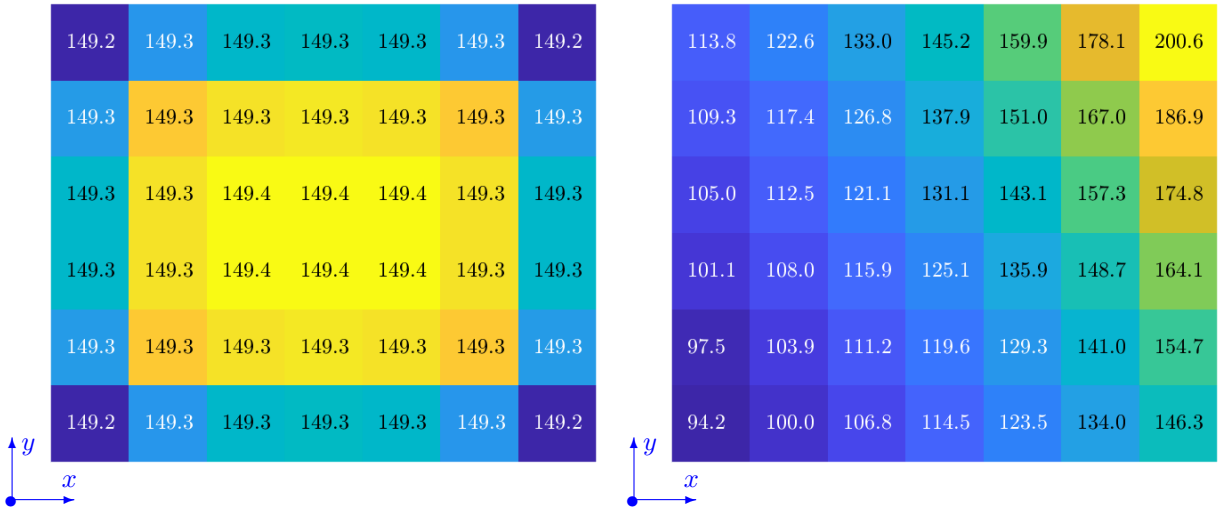

Figure 11: Distribution of the C_0 values (in nF) for (a) the periodic plate and (b) the variable thickness plate of section 5.2.

of I and I_p are computed with respect to the mid-surface of the plate:

$$I(y) \quad = \int_0^a \int_{-h_\mathrm{s}/2}^{h_\mathrm{s}/2} z^2 \, dx \, dz, \tag{22a}$$

$$I_\mathrm{p}(y) \quad = \int_{(a-l_\mathrm{p})/2}^{(a+l_\mathrm{p})/2} \int_{h_\mathrm{s}/2}^{h_\mathrm{s}/2+h_\mathrm{p}} z^2 \, dx \, dz. \tag{22b}$$

Similar equations can be written to estimate the bending stiffness $K_{\theta x}^E$ when x is deemed as the normal axis.

In the case of a periodic plate, the thickness $h_\mathrm{s}(x, y)$ does not depend on the (x, y) coordinates, as opposed to what is drawn in figure 10. Then computing the bending stiffness along both in-plane directions give the same result:

$$K_\theta^E = K_{\theta x}^E = K_{\theta y}^E. \tag{23}$$

4.3. Estimation of the static piezoelectric capacitance

The free piezoelectric capacitance, usually denoted C^σ, is the capacitance obtained under zero stress. This value can be estimated by using the relative permittivity ϵ_{33}^σ in table 2. However, this quantity is notably different from the static capacitance C_0 that appears in equation (19). Indeed, the piezoelectric patches are not entirely free to move since they are bound to the structure. Another way of estimating C_0 involves computing the dynamic capacitance $C^{(\mathrm{j})}(\Omega)$:

$$C^{(\mathrm{j})}(\Omega) = \frac{Q^{(\mathrm{j})}}{V^{(\mathrm{j})}}. \tag{24}$$

The piezoelectric capacitance is frequency-dependent because of the piezoelectric coupling. It has been explained in [41] and [42], among others. The j-th static capacitance C_0 would then be equal to $C^{(\mathrm{j})}(\Omega)$ at 0 Hz.

A simulation of $C^{(\mathrm{j})}(\Omega)$ can be obtained by using the finite element formulation of equation (7). When considering the j-th piezoelectric patch, $V^{(\mathrm{j})}$ serves as the excitation. Meanwhile, the other patches are left in open-circuit, which means all values in $\mathbf{Q}$ are set to 0 except $Q^{(\mathrm{j})}$. The C_0 values distribution for the constant thickness plate previously studied is exhibited in figure 11a. One can notice that the boundary conditions have an influence on the static capacitances, as the C_0 values are smaller in the corners than at the center. However, a reasonable assumption is to set $C_0 = 149.3$ nF for all piezoelectric patches of the plate.

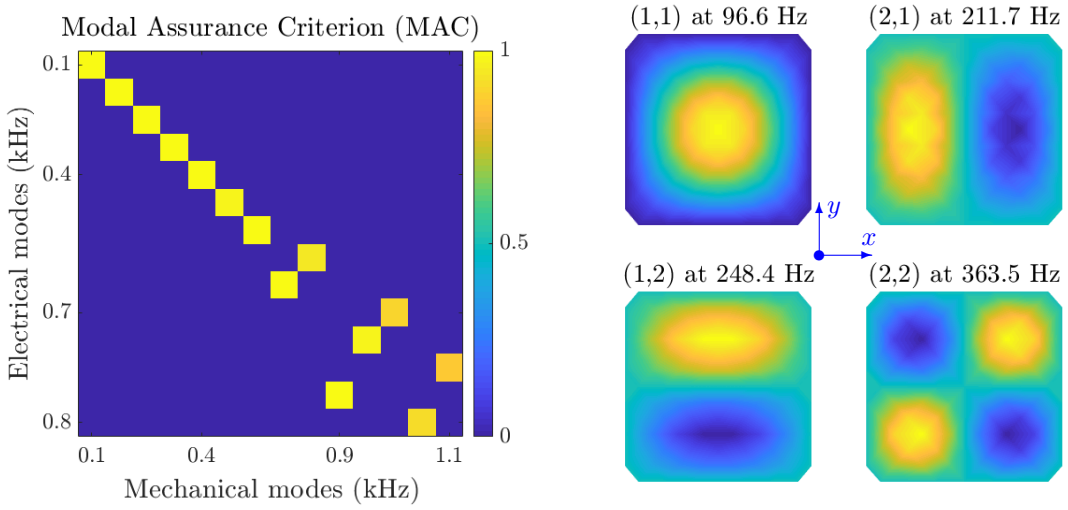

(a) (b)

Figure 12: (a) MAC matrix between simulated electrical current modes of the network and simulated velocity modes of the periodic plate. (b) First four modes of the periodic plate electrical analogous network.

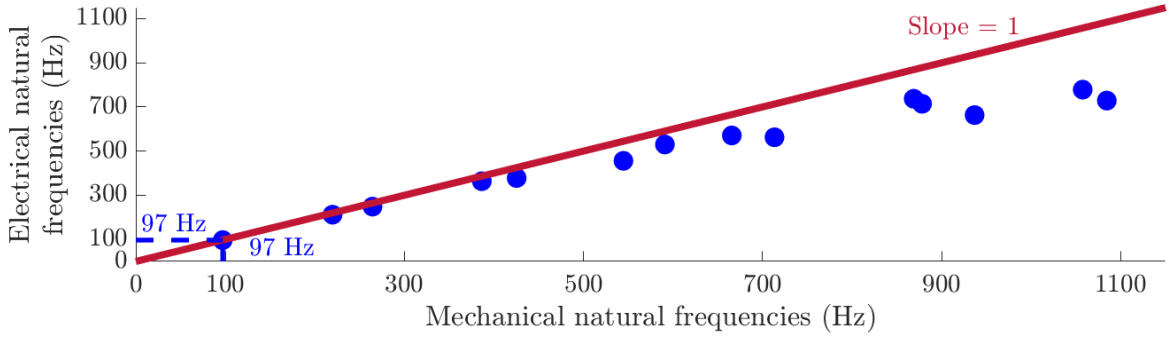

Figure 13: Comparison of the simulated natural frequencies of the periodic plate and of its electrical analogous network.

4.4. Network validation and broadband damping

Now that the parameters K_θ^E and C_0 have been estimated, the inductance value L can be derived for each unit cell of the network by applying the frequential coherence condition of equation (19). The resulting value is 246.6 mH. As stated in section 2.2, the produced inductors have a nominal inductance value of 244 mH, which is close enough to the targeted value to attain a significant damping performance in the end.

Since their behaviors can be predicted, the analogy between the plate and the network can be verified by comparing the mode shapes and the natural frequencies of both systems. These comparisons are quite important since they are the main verification methods that will be available in future numerical examples. The MAC can be used in this case as well, to check if there is a similarity between electrical and mechanical mode shapes. The MAC matrix of the plate and its analogous network is represented in figure 12a, while the simulated natural frequencies of both systems are compared in figure 13. The MAC matrix shows that the first fourteen electrical and mechanical mode shapes are mutually consistent, and the comparison of natural frequencies shows that both systems have the same first natural frequencies. The fact that the MAC matrix is not diagonal is due to the comparison between results obtained with a lumped model on one hand,

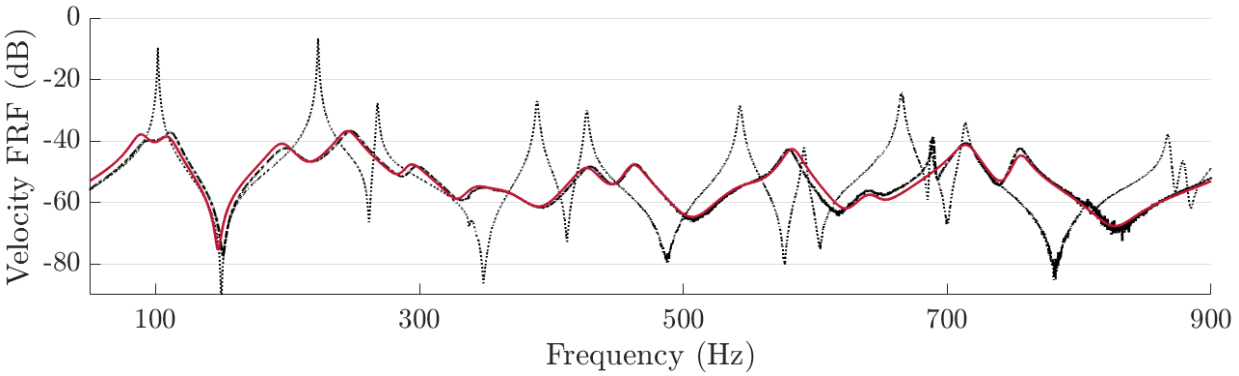

Figure 14: Comparison of velocity FRFs : $(\cdots)$ experimental FRF measured with the piezoelectric patches in short-circuit, $(- \cdot -)$ experimental and (—) simulated FRF when the periodic plate is connected to its electrical analogous network.

and with a finite element model on the other hand. Discretizing the electrical network with more unit cells would make the MAC matrix tend to a diagonal matrix, and would bring mechanical and electrical natural frequencies closer. In the end, these figures are further arguments in showing that the developed network is an electrical analogue of the plate over the considered frequency range.

The case of the structure being coupled to its passive electrical analogue is finally considered. As seen in figure 14, broadband vibration damping is achieved. Meanwhile, the frame mode at 687 Hz is barely affected by the connection to the network, which was expected. Besides, the model in equation (13) is able to predict the dynamics of the structure coupled to its electrical analogue. Hence, this model could be used to find the optimal resistive components to be added to the network in order to numerically optimize the damping performance.

5. Broadband damping of non-periodic plates

The present objective is to extend the concept of piezoelectric network damping to complex structures. The two complex cases studied in this section are non-periodic plates. The first one has a mass locally added on its surface. The second one is a plate of varying thickness. In both cases, the parameters of the frequential coherence condition are estimated. The plate analogues are then validated by comparing the natural frequencies and mode shapes of the structures and of the networks. Finally, a promising broadband vibration damping performance is achieved by coupling the plates to their respective analogous networks.

5.1. Plate with an additional local mass

The first case of a complex plate here treated is the addition of a mass which is a 22 mm thick, 40 mm diameter cylindrical rod of 207 g. This mass is added on the side of the plate which is not covered by piezoelectric patches, on the crossed position in figure 6. The mass is added in the finite element model as well, in the form of a 22 mm thick patch covering the same surface as a piezoelectric patch. Its Young modulus is set at 325 MPa. This way, the seventh simulated natural frequency of the plate with short-circuited patches is adjusted to the seventh peak on the measured FRF. Moreover, the damping coefficient ξ of equation (14) is now set at 6.10^{-3} so that the amplitude of the seventh simulated peak is roughly equal to the measured one. The correlation between numerical and experimental results in this case is shown in figure 17. When compared to the results in figure 8, one can notice that the natural frequencies of the plate have been lowered, that the contact with the added mass induces damping in the measured FRF, and that a frame mode at 203 Hz is now observed. Since the frame is not modeled, its effects can not be foreseen. The simulated FRF fits quite well with the measured one nonetheless.

To define the non-periodic plate electrical analogue, the first idea is to keep using the frequential coherence condition of equation (19). Since the mass m has locally been multiplied by a factor of around 6.2, a first

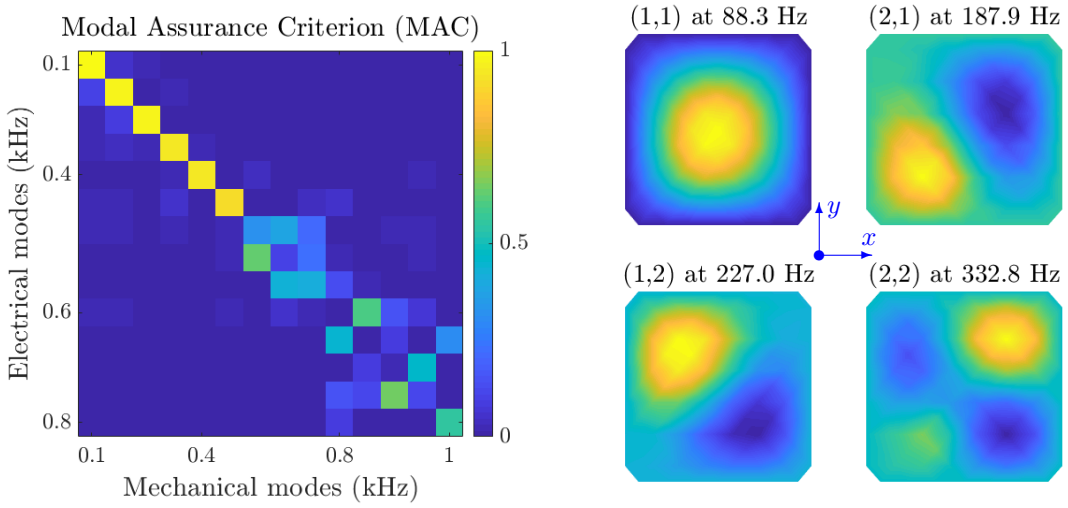

(a) (b)

Figure 15: (a) MAC matrix between simulated electrical current modes of the modified network and simulated velocity modes of the plate on which a mass has been added. (b) First four modes of the electrical network with a local modification of inductance.

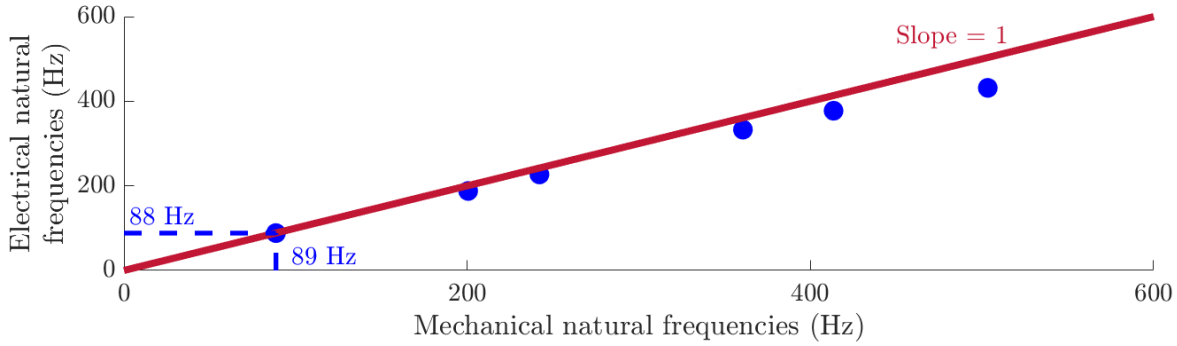

Figure 16: Comparison of the simulated natural frequencies of the periodic plate on which a mass has been added and of its electrical analogous network.

approximation would be to multiply the product LC_0 of the corresponding unit cell by the same factor. If only L is modified not to deteriorate the electromechanical coupling [9], the new inductance value would be $6.2 \times 246.6 = 1.53$ H. This value is an overestimation however, as some mechanical stiffness is locally added as well. In this particular studied case, we propose not to use the frequential coherence condition of equation (19) to define the electrical analogue. Indeed, modeling the contact of the added mass on the plate to estimate the locally added stiffness is out-of-scope of this work. Furthermore, the stiffness model drawn in figure 10 gives correct results only if the mid-surface of the unit cell is close to the mid-surface of the plate. This is not the case here, since the added mass is nearly seven times thicker than the plate. Thus, we suggest to define the non-periodic plate electrical analogue by tuning the first natural frequency of the electrical network to the first natural frequency of the non-periodic plate. The first simulated resonance at around 88 Hz in figure 17 is used as a reference value for the structure. Numerical simulations show that the initial inductance of 246.6 mH should be locally replaced by an inductance of 1.34 H to set the first natural frequency of the network to around 88 Hz.

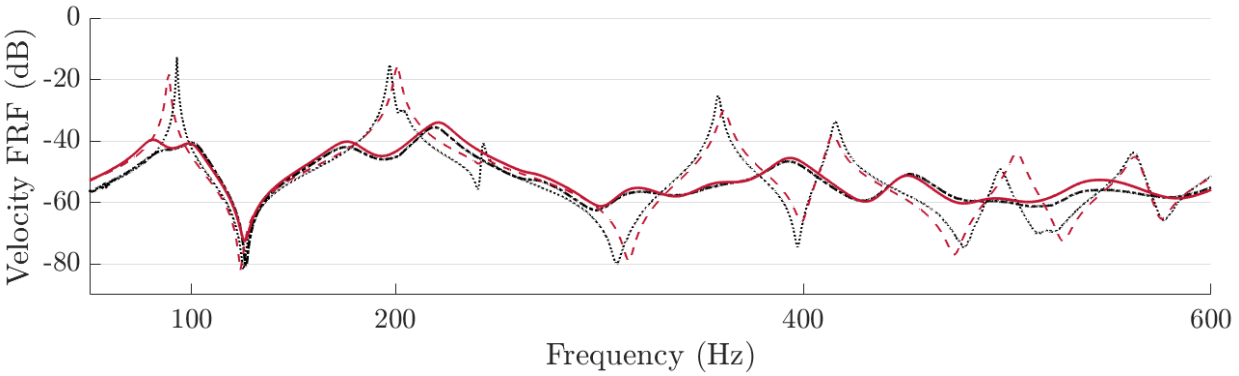

Figure 17: Comparison of velocity FRFs with the added mass: $(\cdots)$ experimental and $(--)$ simulated FRF measured with the piezoelectric patches in short-circuit, $(- \cdot -)$ experimental and $(—)$ simulated FRF when the plate on which a mass had been added is connected to its electrical analogous network.

The electrical current mode shapes of the modified network are computed using the model of equation (5). The mode shapes of the periodic plate represented in figure 12b are different from those seen in figure 15b, which are not symmetric anymore. They are then compared to the velocity modes of the mechanical structure, which are computed using equation (6). The MAC between these set of natural vectors is plotted in figure 15a, and the comparison of mechanical and electrical natural frequencies is made in figure 16. It shows that the first six modes of the network and of the plate are mutually consistent. To obtain a proper analogy at higher frequencies, two solutions are possible. The first one would be to have more piezoelectric patches on the plate, which is equivalent to refine the meshing of the analogous network. The second solution would be to find another analogous unit cell for the plate. Indeed, the significant mass discontinuity induced by the added mass can hardly be predicted by a finite difference model. As a consequence, this studied case can be deemed as the limit case of validity for the plate electrical analogue of section 2. In the end, the analogy between the non-periodic plate and the modified network is still verified up to around 600 Hz.

The non-periodic plate is now coupled to its passive electrical analogue. The FRF measurement is made with the same setup as described in section 3.3. As seen in figure 17, broadband damping is achieved in this case as well. This result validates the approach of coupling a non-periodic structure to its fully passive electrical analogue for multimodal damping purposes. Besides, the simulated results fit rather well with the measured ones. The remaining differences are due to the differences already spotted between results with short-circuited piezoelectric patches, and hence could be reduced by modeling the non-ideal boundary conditions. As it is, this shows that the finite element model developed in this work and expressed by equation (13) can be used to predict the dynamics of a complex structure coupled to an electrical network. It could also be used to design the dissipative components that could be added in the network to improve the damping performance.

5.2. Variable thickness plate

The last studied case is a plate with the same geometry and dimensions as in figure 6 but with a variable thickness. For now, it is assumed that the thickness h_s of the plate varies linearly with the x and y coordinates. Therefore, with α, β, γ and δ being real values:

$$h_\mathrm{s}(x, y) = \alpha + \beta x + \gamma y + \delta xy. \tag{25}$$

The numerical values of h_s at the plate corners are summed up in table 3. The thickness of each piezoelectric patch is constant and is set at 1/6 of the mean thickness of the plate portion it covers.

The frequential coherence condition (19) should still be locally verified to ensure that the structure and its analogous network have identical bending wave propagation properties. The choice is to use the inductance value L as the tuning parameter. As stated previously, the square unit cell is still of side $a = 60$

Table 3: Thicknesses values at the corners of the plate. These four values are enough to set the profile of the plate such as defined in equation (25).

Position x (mm)	Position y (mm)	Thickness $h_s(x, y)$ (mm)
0	0	5
420	0	3
0	360	4
420	360	2

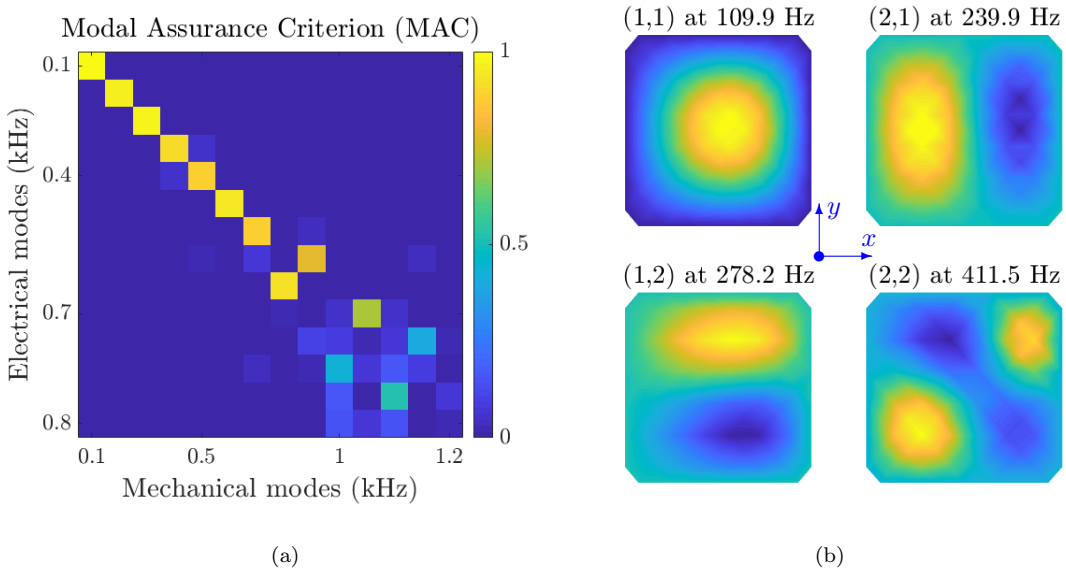

(a) (b)

Figure 18: (a) MAC matrix between simulated electrical current modes of the network and simulated velocity modes of the variable thickness plate. (b) First four modes of the variable thickness plate electrical analogous network.

mm. The transformer ratio is kept at $\hat{a} = 4$. The local values of m can be computed knowing the thickness $h_s(x, y)$ variations and the materials densities, which remain the same as before. This means that K_θ^E and C_0 should be estimated to obtain a value for L.

Because of the thickness variations, the bending stiffness $K_{\theta x}^E$ and $K_{\theta y}^E$ along the in-plane directions have two different values. Estimating these quantities by using the model drawn in figure 10 is made by replacing h_s by its formulation of equation (25) in the method detailed in section 4.2. In the end, the stiffness in equation (19) is taken as the mean value of $K_{\theta x}^E$ and $K_{\theta y}^E$:

$$K_\theta^E = \frac{1}{2}\left(K_{\theta x}^E + K_{\theta y}^E\right). \tag{26}$$

As far as the static capacitances distribution go, the same method as suggested in section 4.3 is followed. The resulting C_0 values distribution obtained with the finite element model of equation (7) is shown in figure 11b. The comparison with the case of a periodic plate shows that all C_0 values are different from one another in the present case since all piezoelectric patches have different thicknesses.

Now that the parameters K_θ^E and C_0 have been estimated, the inductance value L can be derived for each unit cell of the network by applying the frequential coherence condition of equation (19). Calculating the MAC and comparing mechanical and electrical natural frequencies are the main methods of analogy validation that are going to be used going towards even more complex structures. Hence we use it here

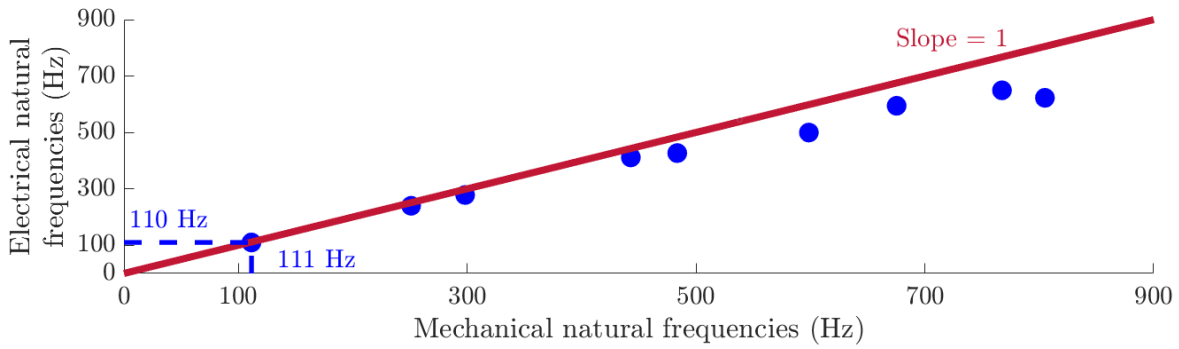

Figure 19: Comparison of the simulated natural frequencies of the variable thickness plate and of its electrical analogous network.

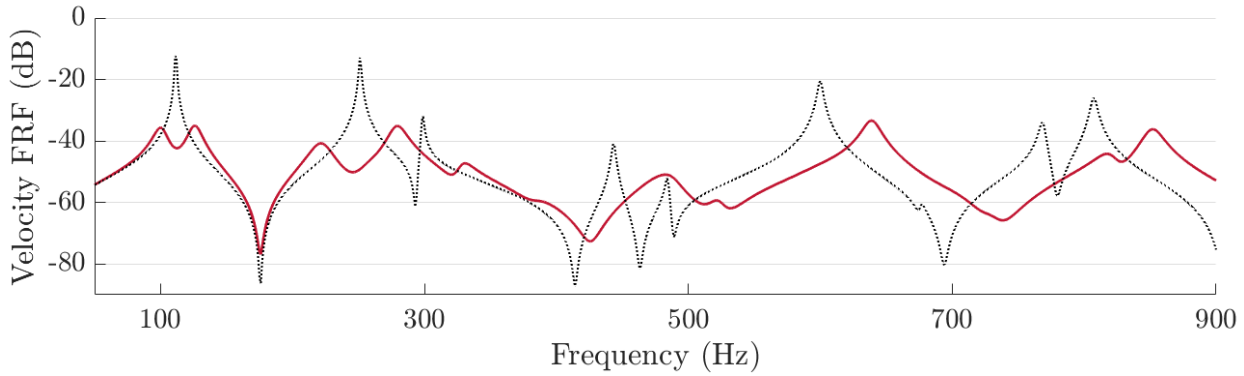

Figure 20: (···) Simulated FRF with the piezoelectric patches in short-circuit, and (—) simulated FRF when the variable thickness plate is connected to its electrical analogous network.

to check that the developed network is the electrical analogue of the considered non-periodic plate. The mode shapes and natural frequencies of the network and of the non-periodic plate are compared in figure 18 and 19, respectively. The analogy between the two systems is ensured up to the tenth electrical current mode, which is promising for broadband vibration damping.

The behavior of the plate of variable thickness being coupled to its electrical analogue is finally simulated using the finite element formulation of equation (13). The excitation is applied to the plate surface where the piezoelectric patches are bound, at the same point as drawn in figure 6. The same non-ideal transformers as described in section 2.2 are considered to add some damping to the coupled system. However, the series resistances of the inductors are set to 0, as it allows better perception of the tuning of the analogous network. The driving-point mobility is plotted in figure 20. It shows that the objective of the designed analogous network is met, as the first few modes of the variable thickness plate are damped thanks to the piezoelectric coupling with the analogous network. While resistors could be included in the model in different positions of the network in order to enhance the damping performance, this validates the effectiveness of the damping solution here proposed. Moreover, the electrical components characteristics are realistic. This highlights the feasibility of integrating such a broadband damping solution with purely passive components to a complex structure.

6. Conclusions

This work investigates the extension of piezoelectric network damping to non-periodic structures. Indeed, the efficiency of coupling a periodic mechanical structure via thin piezoelectric patches to a periodic electrical

network for passive broadband damping purposes has been proven before. The process followed in this article is to start from the known case of a periodic plate and to gradually make it non-periodic. In all situations, the structure is connected to an electrical analogue. The electrical network is designed to exhibit the same modal properties as the mechanical structure to be damped.

As a consequence, the case of a periodic simply-supported plate is first considered. Its electrical analogue is derived by applying the direct electromechanical analogy to a finite difference model of a Kirchhoff-Love square plate. The resulting unit cell is then assembled to create the periodic plate electrical analogue. This network is implemented by producing passive electrical components. The network is then connected to its analogous mechanical structure. Vibration damping of the first eleven modes of the plate, which are spread over a frequency range of nearly 1 kHz, is achieved.

Following this, cases of non-periodic plates are investigated. The first one involves a local mass addition on the plate surface. The natural frequencies and the mode shapes of the structure change because of this addition. The network is modified accordingly, and a significant multimodal vibration damping performance is obtained once again. The second studied case of a non-periodic plate is a plate with a variable thickness. This last case is entirely numerical. The electrical components of the network are designed by respecting the frequential coherence condition previously derived. The final simulations highlight the achievable damping performance with a fully passive electrical network connected to the non-periodic structure. It is a first successful step towards coupling a complex structure to its electrical analogue for multimodal damping purposes.

Meanwhile, a predictive model of the coupled system has been proposed. It involves a finite element model of a mechanical structure covered by thin piezoelectric patches on one hand, and a behavioral system of the electrical network on the other hand. Both models have been validated independently by comparison with experimental results on periodic and non-periodic plates and networks. These two models have then be merged to forecast the electromechanical dynamics of the coupled system, which is a contribution of the present article. This larger model has also been validated by comparison with experimental results on periodic and non-periodic structures. Therefore, one can be confident about using this finite element formulation going towards more complex structures. These structures could be plates with various boundary conditions, arches or tubes. Future works will study the attainable vibration damping performance when these structures are coupled to their respective analogous networks. Furthermore, it is now possible to predict the optimal resistive components to add to the network to optimize the damping performance. To do so, defining quantitative criteria to estimate the multimodal damping performance will be required.

References

[1] N. W. Hagood, A. Von Flotow, Damping of structural vibrations with piezoelectric materials and passive electrical networks, Journal of Sound and Vibration 146 (1991) 243–268.

[2] K. Yamada, H. Matsuhisa, H. Utsuno, K. Sawada, Optimum tuning of series and parallel LR circuits for passive vibration suppression using piezoelectric elements, Journal of Sound and Vibration 329 (2010) 5036–5057.

[3] O. Thomas, J. Ducarne, J.-F. Deü, Performance of piezoelectric shunts for vibration reduction, Smart Materials and Structures 21 (2012) 015008.

[4] J. J. Hollkamp, Multimodal passive vibration suppression with piezoelectric materials and resonant shunts, Journal of Intelligent Material Systems and Structures 5 (1994) 49–57.

[5] S. Wu, Method for multiple mode piezoelectric shunting with single PZT transducer for vibration control, Journal of Intelligent Material Systems and Structures 9 (1998) 991–998.

[6] S. Behrens, S. O. R. Moheimani, A. J. Fleming, Multiple mode current flowing passive piezoelectric shunt controller, Journal of Sound and Vibration 266 (2003) 929–942.

[7] M. Berardengo, S. Manzoni, A. M. Conti, Multi-mode passive piezoelectric shunt damping by means of matrix inequalities, Journal of Sound and Vibration 405 (2017) 287–305.

[8] J. Ducarne, O. Thomas, J.-F. Deü, Placement and dimension optimization of shunted piezoelectric patches for vibration reduction, Journal of Sound and Vibration 331 (2012) 3286–3303.

[9] A. J. Fleming, S. Behrens, S. O. R. Moheimani, Reducing the inductance requirements of piezoelectric shunt damping systems, Smart Materials and Structures 12 (2003) 57–64.

[10] A. Spadoni, M. Ruzzene, K. Cunefare, Vibration and wave propagation control of plates with periodic arrays of shunted piezoelectric patches, Journal of Intelligent Material Systems and Structures 20 (2009) 979–990.

[11] F. Casadei, M. Ruzzene, L. Dozio, K. A. Cunefare, Broadband vibration control through periodic arrays of resonant shunts: experimental investigation on plates, Smart Materials and Structures 19 (2009) 015002.

[12] S. Vidoli, F. dell'Isola, Modal coupling in one-dimensional electromechanical structured continua, Acta Mechanica 141 (2000) 37–50.
[13] C. Maurini, F. dell'Isola, D. D. Vescovo, Comparison of piezoelectronic networks acting as distributed vibration absorbers, Mechanical Systems and Signal Processing 18 (2004) 1243–1271.
[14] F. dell'Isola, C. Maurini, M. Porfiri, Passive damping of beam vibrations through distributed electric networks and piezoelectric transducers: prototype design and experimental validation, Smart Materials and Structures 13 (2004) 299–308.
[15] P. Bisegna, G. Caruso, F. Maceri, Optimized electric networks for vibration damping of piezoactuated beams, Journal of Sound and Vibration 289 (2006) 908–937.
[16] I. Giorgio, L. Galantucci, A. D. Corte, D. D. Vescovo, Piezo-electromechanical smart materials with distributed arrays of piezoelectric transducers: current and upcoming applications, International Journal of Applied Electromagnetics and Mechanics 47 (2015) 1051–1084.
[17] S. Alessandroni, F. dell'Isola, M. Porfiri, A revival of electric analogs for vibrating mechanical systems aimed to their efficient control by PZT actuators, International Journal of Solids and Structures 39 (2002) 5295–5324.
[18] A. Bloch, Electromechanical analogies and their use for the analysis of mechanical and electromechanical systems, Journal of the Institution of Electrical Engineers - Part I: General 92 (1945) 157–169.
[19] L. L. Beranek, Acoustics, Acoustical Society of America, 1954.
[20] R. H. MacNeal, The solution of partial differential equations by means of electrical networks, Ph.D. thesis, California Institute of Technology, 1949.
[21] S. U. Benscoter, R. H. MacNeal, Introduction to electrical-circuit analogies for beam analysis, NACA Technical Note 2785 (1952).
[22] S. U. Benscoter, R. H. MacNeal, Equivalent-plate theory for a straight multicell wing, NACA Technical Note 2786 (1952).
[23] U. Andreaus, F. dell'Isola, M. Porfiri, Piezoelectric passive distributed controllers for beam flexural vibrations, Modal Analysis 10 (2004) 625–659.
[24] M. Porfiri, F. dell'Isola, F. M. F. Mascioli, Circuit analog of a beam and its application to multimodal vibration damping, using piezoelectric transducers, International Journal of Circuit Theory and Applications 32 (2004) 167–198.
[25] M. Porfiri, F. dell'Isola, E. Santini, Modeling and design of passive electric networks interconnecting piezoelectric transducers for distributed vibration control, International Journal of Applied Electromagnetics and Mechanics 21 (2005) 69–87.
[26] S. Alessandroni, U. Andreaus, F. dell'Isola, M. Porfiri, Piezo-ElectroMechanical (PEM) Kirchhoff–Love plates, European Journal of Mechanics - A/Solids 23 (2004) 689–702.
[27] S. Alessandroni, U. Andreaus, F. dell'Isola, M. Porfiri, A passive electric controller for multimodal vibrations of thin plates, Computers & Structures 83 (2005) 1236–1250.
[28] B. Lossouarn, J.-F. Deü, M. Aucejo, Multimodal vibration damping of a beam with a periodic array of piezoelectric patches connected to a passive electrical network, Smart Materials and Structures 24 (2015) 115037.
[29] B. Lossouarn, J.-F. Deü, M. Aucejo, K. A. Cunefare, Multimodal vibration damping of a plate by piezoelectric coupling to its analogous electrical network, Smart Materials and Structures 25 (2016) 115042.
[30] B. Lossouarn, M. Aucejo, J.-F. Deü, K. A. Cunefare, Design of a passive electrical analogue for piezoelectric damping of a plate, Journal of Intelligent Material Systems and Structures (2017) 1045389X1773123.
[31] A. Benjeddou, Advances in piezoelectric finite element modeling of adaptive structural elements: a survey, Computers & Structures 76 (2000) 347–363.
[32] J. Mackerle, Smart materials and structures—a finite element approach—an addendum: a bibliography (1997–2002), Modelling and Simulation in Materials Science and Engineering 11 (2003) 707–744.
[33] O. Thomas, J.-F. Deü, J. Ducarne, Vibrations of an elastic structure with shunted piezoelectric patches: efficient finite element formulation and electromechanical coupling coefficients, International Journal for Numerical Methods in Engineering 80 (2009) 235–268.
[34] B. Lossouarn, M. Aucejo, J.-F. Deü, B. Multon, Design of inductors with high inductance values for resonant piezoelectric damping, Sensors and Actuators A: Physical 259 (2017) 68–76.
[35] R. J. Allemang, The modal assurance criterion - twenty years of use and abuse, Sound & vibration 37 (2003) 14–23.
[36] A. A. Ozdemir, S. Gumussoy, Transfer function estimation in system identification toolbox via vector fitting, IFAC-PapersOnLine 50 (2017) 6232–6237.
[37] B. Lossouarn, M. Aucejo, J.-F. Deü, Electromechanical wave finite element method for interconnected piezoelectric waveguides, Computers & Structures 199 (2018) 46–56.
[38] PI Ceramic, Piezoelectric ceramic products: Fundamentals, characteristics and applications, 2016.
[39] O. Robin, J.-D. Chazot, R. Boulandet, M. Michau, A. Berry, N. Atalla, A plane and thin panel with representative simply supported boundary conditions for laboratory vibroacoustic tests, Acta Acustica united with Acustica 102 (2016) 170–182.
[40] L. Rouleau, B. Lossouarn, R. Darleux, J.-F. Deü, Comparison of damping performances of constrained viscoelastic layers and passive piezoelectric networks, in: 48th International Congress and Exposition on Noise Control Engineering, INTERNOISE 2019, Madrid, Spain, 2019. URL: https://hal.archives-ouvertes.fr/hal-02238171.
[41] A. Preumont, Vibration Control of Active Structures, 3rd ed., Springer Netherlands, 2011. URL: http://www.ebook.de/de/product/19293363/a_preumont_vibration_control_of_active_structures.html.
[42] M. Berardengo, O. Thomas, C. Giraud-Audine, S. Manzoni, Improved resistive shunt by means of negative capacitance: new circuit, performances and multi-mode control, Smart Materials and Structures 25 (2016) 075033.